

Homotopy classification of knotted defects in bounded domains

Yuta Nozaki^{1,4}, David Palmer², and Yuya Koda^{3,4}

¹Faculty of Environment and Information Sciences, Yokohama National University, Yokohama 240-8501, Japan; nozaki-yuta-vn@ynu.ac.jp

²School of Engineering and Applied Sciences, Harvard University, Cambridge, Massachusetts 02138, USA; dpalmer@seas.harvard.edu

³Department of Mathematics, Hiyoshi Campus, Keio University, Yokohama 223-8521, Japan; koda@keio.jp

⁴International Institute for Sustainability with Knotted Chiral Meta Matter (WPI-SKCM²), Hiroshima University, 1-3-1 Kagamiyama, Higashi-Hiroshima, Hiroshima 739-8526, Japan

Abstract

Nozaki et. al. gave a homotopy classification of the knotted defects of ordered media in three-dimensional space by considering continuous maps from complements of spatial graphs to the order parameter space modulo a certain equivalence relation. We extend their result by giving a classification scheme for ordered media in handlebodies, where defects are allowed to reach the boundary. Through monodromies around meridional loops, global defects are described in terms of planar diagrams whose edges are colored by elements of the fundamental group of the order parameter space. We exhibit examples of this classification in octahedral frame fields and biaxial nematic liquid crystals.

1 Introduction

The relationship between ordered media and their topological defects is a central object of study in condensed matter physics. Though the classification of individual defects via homotopy theory has been understood for decades [23, 22, 17, 18, 29], the global classification of defect *configurations* in three dimensions remains a challenge. To put it simply, the problem is, given a pair of defect configurations, to determine whether they are equivalent under transformations arising from the physical evolution of the underlying order parameter field. These allowed transformations include, at a minimum, isotopy of the defects.

The most-studied case is that of *nematic* symmetry, as observed in liquid crystals. For three-dimensional nematics, the order parameter space is $\mathbb{R}P^2$, which has fundamental group $\mathbb{Z}_2 = \mathbb{Z}/2\mathbb{Z}$. For individual line defects, this is perhaps the simplest possible case. However, the search for a global classification is made more complicated by the fact that $\pi_2(\mathbb{R}P^2)$ is non-zero [15, 16]. More-exotic ordered media, such as the hypothetical biaxial nematics [28], feature defect lines classified by elements of a non-abelian group. This renders the global classification problem more difficult—for one thing, individual defect labels are only defined up to conjugation.

Outside of soft-matter physics, non-abelian topological defect configurations arise in the hexahedral meshing problem in geometry processing and computational engineering. This is the problem of decomposing a domain in \mathbb{R}^3 into topological cubes satisfying certain combinatorial conditions. Following related work in two dimensions, [19] proposed a method for hexahedral meshing of volumes by first computing an octahedral bundle with defects (known in the meshing literature as singularities). Such a bundle can be encoded by an order parameter field with octahedral symmetry, a so-called *octahedral frame field* [9] (see Figure 1 and Appendix B). To that end, a line of research in geometry processing has studied discretizing, parametrizing, and optimizing such fields [12, 10, 26, 24, 3, 21, 6].

However, some octahedral field defect configurations are known to be incompatible with hexahedral meshing, necessitating the development of algorithms to correct singularity graphs and associated frame fields [14, 5, 13, 4]. Thus far these methods only operate at the level of individual defect lines. As such, they cannot guarantee global meshability, i.e., the realizability of a defect configuration in a hexahedral mesh. To make theoretical progress on this problem would require a better understanding of the global topology of defect configurations in both the field and mesh settings.

In applications to both liquid crystal physics and meshing, interactions between defects and the domain boundary are significant. Experimentalists have used anchoring of liquid crystals to

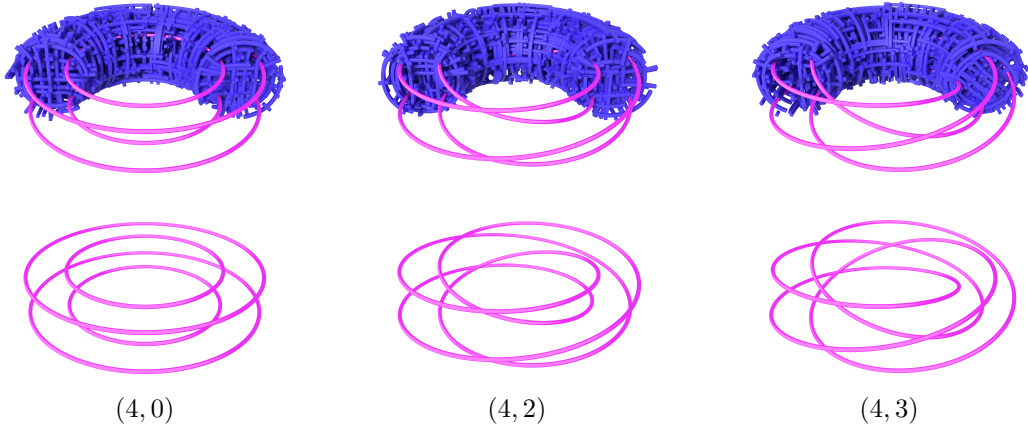


Figure 1: Integral curves and defects of three different octahedral frame fields on the solid torus. Their defects—all of conjugacy class $[(1+i)/\sqrt{2}] \subset 2O$ —form a 4-component unlink (left), a $(4,2)$ -torus link (center), and a $(4,3)$ -torus knot (right).

substrates to control defects [27], interacting colloidal particles [25], and even micro-robots [30]. In meshing, the problem instance is specified by the boundary geometry, and correct discretization of the boundary is vitally important for downstream applications of hexahedral meshes. Despite these practical considerations, boundary conditions complicate the classification of defect configurations, and most existing work on classification has focused on the boundary-free setting, i.e., defects in the 3-sphere.

Topological invariants that distinguish global defect configurations have been proposed in [8, 2, 1]. However, these invariants are not known to be sufficient to completely classify configurations. To our knowledge, the first work in that direction is by Nozaki et al. [20], who give a homotopy classification of knotted defects either in the Euclidean space \mathbb{R}^3 , the 3-sphere S^3 , or the closed 3-ball.

The present work marks a first step toward a global classification in domains with boundary. We extend the tools of [20] to the setting of defects in unknotted handlebodies, subject to some boundary conditions. More precisely, we first formulate a mathematical model for ordered media with defects on a handlebody with boundary conditions and homotopical equivalence relations between them. We then define certain algebraic data derived from the defect configurations. On the other hand, the equivalence classes of ordered media can be described using *colored diagrams* and their moves. Our main result, Theorem 3.4, gives natural bijective correspondences between ordered media with boundary conditions modulo equivalence; colored diagrams up to moves; and the algebraic data. This allows us to classify defect configurations modulo equivalence using purely algebraic data that can be derived from their diagrams.

For concreteness, we illustrate our classification in the case of a biaxial nematic system on the solid torus $M := D^2 \times S^1$ in Appendix A. The order parameter space of that system is S^3/Q , where $Q = \{\pm 1, \pm i, \pm j, \pm k\}$ is the *quaternion group*, and the fundamental group of the boundary ∂M of M , which is a torus, is the free abelian group generated by two loops α and β called the *longitude* and *meridian*, respectively. If we restrict our interest to systems without boundary defects, and further, if we impose a boundary condition that the restriction $f_0: \partial M \rightarrow S^3/Q$ satisfies $(f_0)_*(\alpha) = i \in Q$, then any such system is equivalent to exactly one of the twelve models depicted in Figure 2, whose defect graphs are indicated in black and labeled with monodromies around edges.

Our model can address both ordered media within 3-dimensional handlebodies and ordered media on the exteriors of unknotted handlebodies in the 3-dimensional Euclidean space \mathbb{R}^3 , where the order parameter remains constant at large distances from the origin (see Remark 4.3). We leave to future work the extension of these ideas to more general subspaces of \mathbb{R}^3 and less-restrictive boundary conditions (see Remark 3.2).

Outline. The structure of the paper is as follows. Section 2 reviews prior work on the classification of knotted defects in unbounded domains, following a brief introduction of fundamental tools from algebraic topology that will be used in this paper. Section 3 develops a mathematical model of ordered media up to homotopy in bounded domains, describes their diagrammatic representation, and introduces a certain algebraic invariant. Section 4 presents the main result, offering a complete classification of defect configurations up to equivalence, along with a simple illustrative example. Section 5 gives the proof of the main theorem. Appendix A offers concrete examples illustrating the

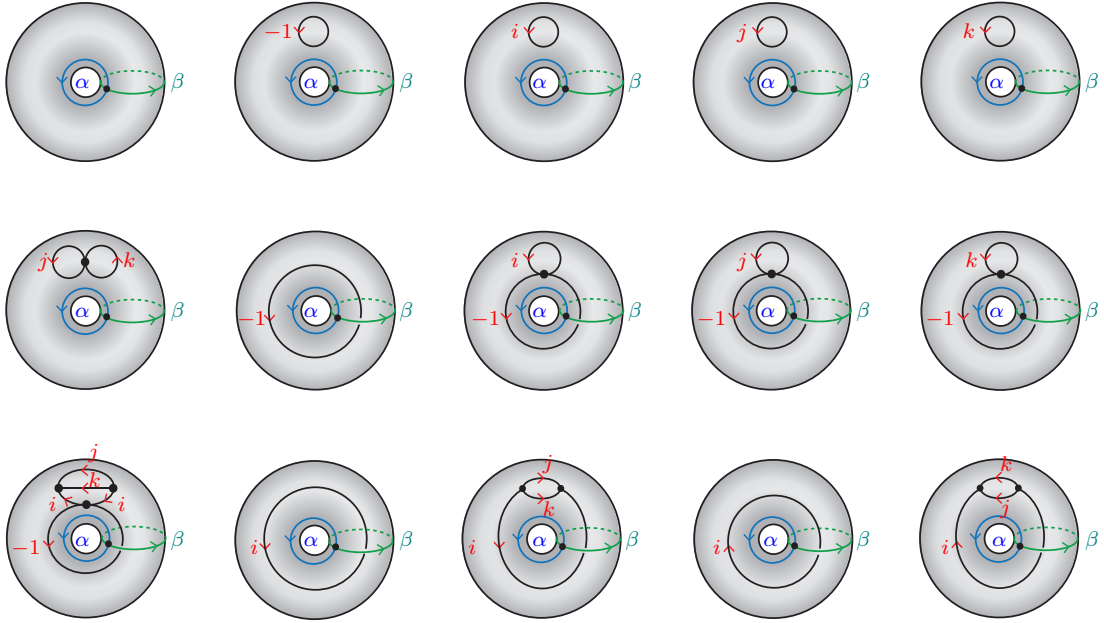


Figure 2: A complete list of defect configurations, up to homotopy, of the biaxial nematic system on the solid torus without boundary defects and subject to the condition that the map $f_0: \partial M \rightarrow S^3/Q$ defined for the system satisfies $(f_0)_*(\alpha) = i \in Q$.

classification process using the main theorem. Appendix B presents a classification of subgroups of the binary octahedral group $2O$ and their conjugacy classes, which can be used for the classification of octahedral frame fields.

Acknowledgments

The authors would like to thank Ivan I. Smalyukh, Tamás Kálmán, and Shun Wakatsuki for valuable discussion. Author Y. Nozaki was supported by JSPS KAKENHI Grant Numbers JP20K14317, JP23K12974 and JP24H00686. Author D. Palmer was supported by NSF MSPRF Grant Number 2303403. Author Y. Koda was supported by JSPS KAKENHI Grant Numbers JP20K03588, JP21H00978, JP23H05437 and JP24K06744.

2 Preliminaries

In this section, we establish the basic notation and mathematical background that will be used in the proof of our main result.

2.1 Groups and their presentations

We recall some basic definitions and facts about groups. Let G be a group with identity element 1 , and let S be a subset of G . We denote by $\langle S \rangle$ the subgroup of G generated by S ; that is, $\langle S \rangle$ is the subgroup of all elements of G that can be expressed as finite products of elements in S . Let $\langle\langle S \rangle\rangle_G$ denote the *normal closure* of S in G , that is, the smallest normal subgroup of G containing S . We say that G is *finitely generated* if there exists a finite subset $S \subset G$ with $\langle S \rangle = G$. We denote the set of finitely generated subgroups of G by S_G^{fg} .

We say that G has a *presentation* $\langle S \mid R \rangle$ if S is a set, R is a subset of the free group F_S on S , and G is isomorphic to the quotient of F_S by the normal closure $\langle\langle R \rangle\rangle_{F_S}$ of R . Here S and R are called sets of *generators* and *relators*, respectively. Thus, if we regard the set of generators S as a subset of G by the above isomorphism, we have $\langle S \rangle = G$, and R is a set of products of generators, each equal to 1 , that are sufficient to express all relations among the generators. Two subgroups H and H' of a group G are said to be *conjugate* if there exists an element x of G with $xHx^{-1} = H'$.

Let $C_G(S)$ denote the *centralizer* of a subset S of G ; that is, $C_G(S) := \{g \in G \mid \forall s \in S, gs = sg\}$. Given two subgroups H and K of G , the set of *double cosets* $H \backslash G / K$ consists of equivalence classes $[g]$ of elements of G , where $[g] = [g']$ if and only if $h g k = g'$ for some $h \in H$ and $k \in K$.

2.2 Homotopy groups

Recall that the fundamental group $\pi_1(X, x_0)$ of a topological space X with a base point x_0 is defined to be the group of homotopy classes of loops $[0, 1] \rightarrow X$ based at x_0 , where the product of two elements is defined by their concatenation.

For pairs of topological spaces (X, A) and (Y, B) , let $\text{Map}((X, A), (Y, B))$ denote the set of continuous maps $f: X \rightarrow Y$ satisfying $f(A) \subset B$. In particular, fixing base points $x_0 \in X$ and $y_0 \in Y$, the set $\text{Map}((X, \{x_0\}), (Y, \{y_0\}))$ of basepoint-preserving continuous maps is simply denoted by $\text{Map}_0(X, Y)$. Let $\text{Hom}(G, H)$ denote the set of homomorphisms from a group G to H . There is a natural map $\text{Map}_0(X, Y) \rightarrow \text{Hom}(\pi_1(X), \pi_1(Y))$, which takes a map $f: X \rightarrow Y$ to the induced homomorphism $f_*: \pi_1(X, x_0) \rightarrow \pi_1(Y, y_0)$ between the fundamental groups. This map descends to

$$\theta: \text{Map}_0(X, Y)/\simeq \rightarrow \text{Hom}(\pi_1(X), \pi_1(Y)),$$

where \simeq is the equivalence relation of basepoint-preserving homotopy.

Example 2.1. For convenience, we describe a few specific groups relevant to the topology of defects in ordered media. Following [17], these groups arise as fundamental groups of order parameter spaces given as quotients $\text{SO}(3)/H$ of the 3-dimensional rotation group $\text{SO}(3)$ by finite subgroups (point groups) H . In such cases, $\pi_1(\text{SO}(3)/H) = 2H \subset \text{SU}(2)$, a central extension of H by \mathbb{Z}_2 .

- The *quaternion group* $Q = \{\pm 1, \pm i, \pm j, \pm k\}$ is the finite non-abelian group generated by four elements $-1, i, j, k$ such that -1 commutes with other elements and they satisfy $(-1)^2 = 1$ and $i^2 = j^2 = k^2 = ijk = -1$. Note that $Q = 2K$, where K is the *Klein four-group* $\mathbb{Z}_2 \times \mathbb{Z}_2$. The group Q classifies line defects in *biaxial nematics*.
- The *binary tetrahedral group* $2T$ is obtained by adding sixteen elements

$$c^{\pm 1}, c^{\pm 2}, \alpha^{\pm 1}, \alpha^{\pm 2}, \beta^{\pm 1}, \beta^{\pm 2}, \gamma^{\pm 1}, \gamma^{\pm 2}$$

to the quaternion group Q , where $c := \frac{1}{2}(1+i+j+k)$, $\alpha := \frac{1}{2}(1+i-j-k)$, $\beta := \frac{1}{2}(1-i+j-k)$ and $\gamma := \frac{1}{2}(1-i-j+k)$.

- The *binary octahedral group* $2O$ is obtained by adding 24 elements to $2T$:

$$\frac{1}{\sqrt{2}}(\pm 1 \pm i), \frac{1}{\sqrt{2}}(\pm 1 \pm j), \frac{1}{\sqrt{2}}(\pm 1 \pm k), \frac{1}{\sqrt{2}}(\pm i \pm j), \frac{1}{\sqrt{2}}(\pm j \pm k), \frac{1}{\sqrt{2}}(\pm k \pm i).$$

$2O$ classifies line defects in *octahedral frame fields*.

In this way, we have a stratification $Q = 2K \subset 2T \subset 2O$. One can check that every element of Q can be expressed as a product of powers of i and j ; thus, we can write $Q = \langle i, j \rangle$. Similarly, we have $2T = \langle i, c \rangle$ and $2O = \langle c, \frac{1}{\sqrt{2}}(i+j) \rangle$. Note that $\langle i \rangle$ and $\langle j \rangle$ are not conjugate as subgroups of Q , whereas they are conjugate as subgroups of $2T$ (and so of $2O$), for we have $c\langle i \rangle c^{-1} = \langle j \rangle$. See Appendix B for the complete list of subgroups of $2O$ and their conjugacy classes.

For an integer $n \geq 2$, the n th homotopy group $\pi_n(X, x_0)$ is obtained from $\text{Map}_0(S^n, X)$ by considering basepoint-preserving homotopies and a concatenation operation similar to that of π_1 . In contrast to π_1 , these groups are always abelian. See, e.g., Hatcher [7], for more details.

2.3 Wirtinger presentation

Definition 2.2. By a *graph* we mean a finite 1-dimensional CW complex, where 0-cells and 1-cells are called its *vertices* and *edges*, respectively. A subspace Γ of S^3 (or \mathbb{R}^3) is called a *spatial graph* if Γ is ambient isotopic to the union of a finite number of straight line segments, where Γ is endowed with the structure of a graph.

Note that knots and links are examples of spatial graphs. Note also that the same subset of S^3 (or \mathbb{R}^3) admits distinct graph structures, distinguished by vertices of valence two. Two spatial graphs are said to be *equivalent* if they are related by an ambient isotopy preserving the graph structure.

Fix a projection $p: \mathbb{R}^3 \rightarrow \mathbb{R}^2$. A spatial graph $\Gamma \subset \mathbb{R}^3$ is said to be in a *regular position* with respect to p if

- (1) for each point x in \mathbb{R}^2 , the set $p^{-1}(x) \cap \Gamma$ consists of at most two points;

- (2) there are only finitely many points x of \mathbb{R}^2 with $|p^{-1}(x) \cap \Gamma| = 2$; such points x are called *crossings*;
- (3) no vertex of Γ projects to a crossing; and
- (4) each crossing $x \in \mathbb{R}^2$ has a neighborhood $U_x \subset \mathbb{R}^2$ such that the set $p^{-1}(U_x) \cap \Gamma$ consists of two straight line intervals.

When we consider spatial graphs in S^3 instead of in \mathbb{R}^3 , we use the projection $S^3 \rightarrow S^2$ induced from $p: \mathbb{R}^3 \rightarrow \mathbb{R}^2$ by the one-point compactification. Note that every spatial graph can be moved by an isotopy to be in a regular position with respect to p . Let Γ be a spatial graph in a regular position with respect to p . A *diagram* D_Γ of Γ is defined to be the image $p(\Gamma)$ such that at each crossing, the incident arcs are labeled with their relative height (over/under). Thus, a diagram of a spatial graph is a purely combinatorial object consisting of a planar graph on \mathbb{R}^2 with over/under information at some of its vertices. Diagrams of equivalent spatial graphs can be related by a finite sequence of local moves called *Reidemeister moves*, which are illustrated in Figure 10 (in the case of colored diagrams).

Let $\Gamma \subset S^3$ be a spatial graph, and take $x_0 \in S^3 \setminus \Gamma$ as a base point. Then, we can get a finite presentation of the fundamental group $\pi_1(S^3 \setminus \Gamma)$ from a diagram D_Γ as follows. For simplicity, we assume that the diagram is connected. Fix an orientation of each edge of Γ . The diagram of Γ consists of finitely many oriented arcs $\alpha_1, \dots, \alpha_n$, where the endpoints of each α_i are vertices or crossings. For $i = 1, \dots, n$, assign a letter x_i to each oriented arc α_i . At each crossing or vertex c_j ($j = 1, \dots, m$), define a relator r_j following the rule shown in Figure 3, where at each vertex v , $\varepsilon_{i_r} = 1$ (resp. $\varepsilon_{i_r} = -1$) if the r th half-edge incident to v is a tail (resp. head). The

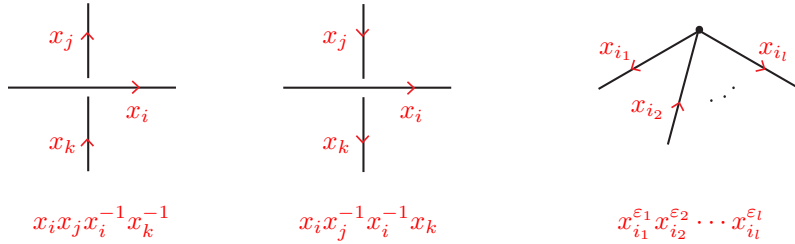


Figure 3: Relators in a Wirtinger presentation.

group $\pi_1(S^3 \setminus \Gamma, x_0)$ then has a presentation $\langle x_1, \dots, x_n \mid r_1, \dots, r_m \rangle$, which is called a *Wirtinger presentation*. In this paper, concatenations of loops in π_1 are read from left to right, the basepoints of all diagrams are above the page, and orientations of meridians follow the right-hand rule. See Kawauchi [11] for more details.

2.4 Review of previous work

We recall the mathematical model of global defect configurations introduced in [20]. Let G be a group, and let X_G be a CW complex satisfying $\pi_1(X_G) \cong G$ and $\pi_2(X_G) = \{0\}$. Note that such a space X_G always exists for any G . Following standard terminology in physics, we refer to X_G as the *order parameter space*.

Fix basepoints $p_0 \in \mathbb{R}^3$ and $x_0 \in X_G$.

Definition 2.3. A *defect configuration* (Γ, f) comprises a spatial graph Γ , the *defect set*, together with an *order parameter field* $f \in \text{Map}_0(\mathbb{R}^3 \setminus \Gamma, X_G)$ defined on the complement of Γ .

We classify defect configurations up to an equivalence relation generalizing homotopy. For defect sets Γ, Γ' and order parameter fields $f \in \text{Map}_0(\mathbb{R}^3 \setminus \Gamma, X_G)$ and $f' \in \text{Map}_0(\mathbb{R}^3 \setminus \Gamma', X_G)$, we say $(\Gamma, f) \sim (\Gamma', f')$, if, after adding finitely many vertices v_i, v'_j and edges e_k, e'_l to each graph, there exists a basepoint-preserving ambient isotopy $\{h_t\}_{t \in [0,1]}$ of \mathbb{R}^3 sending $\widehat{\Gamma} = \Gamma \cup \{v_i\} \cup \{e_k\}$ to $\widehat{\Gamma}' = \Gamma' \cup \{v'_j\} \cup \{e'_l\}$ in such a way that $f|_{\mathbb{R}^3 \setminus \widehat{\Gamma}}$ is homotopic to $f'|_{\mathbb{R}^3 \setminus \widehat{\Gamma}'} \circ h_1$.

Theorem 2.4 ([20]). *The map*

$$\Phi: \left(\coprod_{\Gamma} \text{Map}_0(\mathbb{R}^3 \setminus \Gamma, X_G) \right) / \sim \rightarrow \mathcal{S}_G^{\text{fg}}$$

defined by $\Phi([f]) = \text{Im}(f_*: \pi_1(\mathbb{R}^3 \setminus \Gamma) \rightarrow G)$, is bijective.

3 Mathematical model

Let k be a non-negative integer. A *handlebody* of genus k is a compact orientable 3-manifold with non-empty boundary obtained by attaching k 1-handles to a 0-handle. Note that a handlebody of genus 0 is just a closed 3-ball, while a handlebody of genus 1 is a solid torus $D^2 \times S^1$. See Figure 4. In this section, we extend the mathematical model reviewed in Section 2.4 to cover defects in handlebodies.

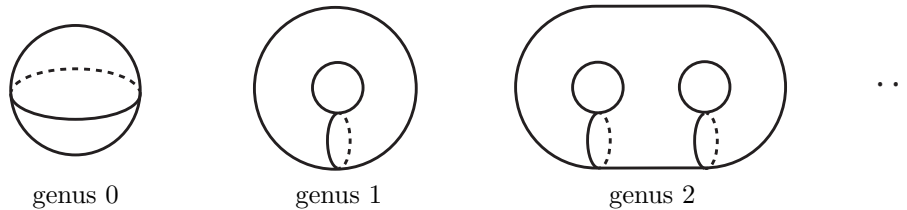


Figure 4: Handlebodies.

Let W be an unknotted handlebody of genus k in S^3 ; that is, a handlebody whose exterior $M = E(W) = S^3 \setminus \text{Int } W$ is also a handlebody. For example, if we regard the handlebodies shown in Figure 4 as embedded in S^3 , then they are unknotted. An unknotted handlebody of genus 1 can be obtained as a regular neighborhood of the unknot, and *knotted* handlebodies of genus 1 can be obtained as regular neighborhoods of non-trivial knots in \mathbb{R}^3 . For convenience, we work on the “unbounded” handlebody M and treat its complement as the exterior.

3.1 Formulation via continuous maps

Fix basepoints $*_{\partial} \in (\partial M) \setminus P$ and $* \in M$ for the boundary and interior, respectively. Also fix a set of *boundary defects* $P = \{p_1, \dots, p_n\} \subset \partial M$ and *boundary values* $f_0 \in \text{Map}_0((\partial M) \setminus P, X_G)$ such that f_0 cannot extend to any p_i .

We consider spatial graphs Γ in $M \setminus \{*\}$ terminating at boundary defects—i.e., satisfying $\partial M \cap \Gamma = P \cap \partial M$. For such a graph, define the associated set of order parameter fields satisfying boundary conditions

$$\text{Map}_0(M \setminus \Gamma, X_G; f_0) = \{f \in \text{Map}_0(M \setminus \Gamma, X_G) \mid f|_{\partial M \setminus P} \text{ is homotopic to } f_0\}.$$

Definition 3.1. We take the total set of defect configurations to be the disjoint union $\coprod_{\Gamma} \text{Map}_0(M \setminus \Gamma, X_G; f_0)$, where Γ runs over spatial graphs as above. We consider two maps $f \in \text{Map}_0(M \setminus \Gamma, X_G; f_0)$ and $f' \in \text{Map}_0(M \setminus \Gamma', X_G; f_0)$ to be *equivalent*, $f \sim f'$, if there exist finitely many vertices $\{v_i\}, \{v'_k\}$ and edges $\{e_j\}, \{e'_l\}$, and a basepoint-preserving ambient isotopy $\{h_t\}_{t \in [0,1]}$ of M , such that:

- h_t restricts to the identity map on ∂M ;
- h_t sends $\widehat{\Gamma} := \Gamma \cup \{v_i\} \cup \{e_j\}$ to $\widehat{\Gamma}' := \Gamma' \cup \{v'_k\} \cup \{e'_l\}$; and
- $f|_{M \setminus \widehat{\Gamma}}$ is homotopic to $f'|_{M \setminus \widehat{\Gamma}'} \circ h_1$ relative to basepoints.

Remark 3.2. The boundary conditions we consider here differ subtly from those that might be more familiar from applications. While in many applications boundary defects are free to move along the boundary, our model strictly fixes the positions of the boundary defects P . In contrast to this strong constraint on boundary defect positions, our treatment of boundary values is relatively loose: we consider them fixed only up to homotopy through the full order parameter space X_G . Some applications feature “anchoring” boundary conditions, which constrain boundary values to a subbundle of the full order parameter bundle. For example, a common condition on nematics or octahedral frames constrains them to align to the boundary normals. Such “subbundle” boundary conditions are inexpressible in our model. Nevertheless, we believe that our model will serve as a bridge to understanding these more familiar boundary conditions as our model is geometrically meaningful and allows complete classification of defect configurations as in the boundary-free case.

Our classification relates defect configurations to subgroups of G augmented with additional data. Given subsets S, S' of G with $S \supset S'$, we write $\mathcal{S}_{G,S,S'}$ for the set of triples $(H, N, [g])$ such that

- (1) H is a subgroup of G , N is a normal subgroup of H , and g is an element of G such that $gSg^{-1} \subset H$ and $gS'g^{-1} \subset N$;

- (2) there exists a finite subset T of N satisfying $\langle gSg^{-1} \cup T \rangle = H$ and $\langle\langle T \rangle\rangle_H = N$; and
- (3) $[g]$ is a double coset represented by g in $N \backslash G / C_G(S)$.

Note that the conditions $gSg^{-1} \subset H$ and $gS'g^{-1} \subset N$ do not depend on the choice of a representative of $[g]$. When G is a finite group, we can drop (2) from the above definition by letting $T = N$.

Intuitively, given a set of boundary monodromies S , the subgroup H encodes all monodromies both around defects and along non-contractible loops on ∂M , the normal subgroup N of H captures only monodromies around interior defects, and $[g]$ records the choice of path connecting the boundary and interior basepoints. The necessity of all three data will be demonstrated explicitly in Example 4.4. Later, we will mainly consider the case where S is a finitely generated subgroup; then (2) implies that H is also finitely generated. In particular, $\mathcal{S}_{G, \{1\}, \{1\}}$ corresponds to $\mathcal{S}_G^{\text{fg}}$ in Section 2.4 since $H = N$ and $[g] = [1]$ for any $(H, N, [g]) \in \mathcal{S}_{G, \{1\}, \{1\}}$.

Example 3.3. Let G be the quaternion group Q , $S = \langle i \rangle = \{\pm 1, \pm i\}$, and $S' = \{1\}$. Let $(H, N, [g])$ be an element of $\mathcal{S}_{Q, \langle i \rangle, \{1\}}$. Since $C_G(S) = C_Q(\langle i \rangle) = \langle i \rangle$, when $N = \langle j \rangle, \langle k \rangle$, or Q , the set $N \backslash Q / C_Q(\langle i \rangle)$ consists of a single coset Q . On the other hand, when $N = \{1\}, \langle -1 \rangle$, or $\langle i \rangle$, the set $N \backslash Q / C_Q(\langle i \rangle)$ consists of exactly two double cosets $[1] = \{\pm 1, \pm i\}$ and $[j] = \{\pm j, \pm k\}$.

Since H should contain a conjugate of $S = \langle i \rangle$, H is $\langle i \rangle$ or Q . When $H = \langle i \rangle$, $(H, N, [g])$ is one of the six elements $(\langle i \rangle, \{1\}, [1])$, $(\langle i \rangle, \{1\}, [j])$, $(\langle i \rangle, \langle -1 \rangle, [1])$, $(\langle i \rangle, \langle -1 \rangle, [j])$, $(\langle i \rangle, \langle i \rangle, [1])$, and $(\langle i \rangle, \langle i \rangle, [j])$; when $H = Q$, $(H, N, [g])$ is one of the three elements $(Q, \langle j \rangle, [1])$, $(Q, \langle k \rangle, [1])$ and $(Q, Q, [1])$. In this way, we can obtain the complete list of elements of $\mathcal{S}_{Q, \langle i \rangle, \{1\}}$. Note that $(Q, \langle i \rangle, [1])$, for example, is not an element of $\mathcal{S}_{Q, \langle i \rangle, \{1\}}$, for we cannot find a subset T of $\langle i \rangle$ satisfying $\langle\langle i \rangle \cup T \rangle = Q$. The following lists of elements of $\mathcal{S}_{Q, \langle i \rangle, \langle -1 \rangle}$ and $\mathcal{S}_{Q, \langle i \rangle, \langle i \rangle}$ can also be obtained in the same way:

$$\begin{aligned} \mathcal{S}_{Q, \langle i \rangle, \langle -1 \rangle} &= \left\{ \begin{array}{l} (\langle i \rangle, \langle -1 \rangle, [1]), (\langle i \rangle, \langle -1 \rangle, [j]), (\langle i \rangle, \langle i \rangle, [1]), (\langle i \rangle, \langle i \rangle, [j]), \\ (Q, \langle j \rangle, [1]), (Q, \langle k \rangle, [1]), (Q, Q, [1]) \end{array} \right\}, \\ \mathcal{S}_{Q, \langle i \rangle, \langle i \rangle} &= \{(\langle i \rangle, \langle i \rangle, [1]), (\langle i \rangle, \langle i \rangle, [j]), (Q, Q, [1])\}. \end{aligned}$$

Let $f \in \text{Map}_0(M \setminus \Gamma, X_G; f_0)$. For each edge e of Γ , let μ_e be a meridian of e , that is, a boundary loop of a sufficiently small disk intersecting e transversely at a point. Connecting μ_e to $*$ defines $f_*(\mu_e)$ up to conjugation in $\text{Im } f_*$; consequently, the normal closure N_f of $\{f_*(\mu_e) \mid e \text{ is an edge of } \Gamma\}$ in $\text{Im } f_*$ is well-defined. Let $N_{\beta\gamma}$ be the normal closure of $\{(f_0)_*(\gamma) \mid \gamma \in \{\beta_1, \dots, \beta_k, \gamma_1, \dots, \gamma_n\}\}$ in $\text{Im}(f_0)_*$, where β_i, γ_j form a subset of basis loops for $\pi_1(\partial M \setminus P)$ as depicted in Figure 5. Intuitively, N_f encodes the monodromies around defects, and $N_{\beta\gamma}$ collects the monodromy data imposed by the boundary conditions on loops that would be contractible in M if not for the defects. Then, we define a map

$$\Phi: \left(\prod_{\Gamma} \text{Map}_0(M \setminus \Gamma, X_G; f_0) \right) / \sim \rightarrow \mathcal{S}_{G, \text{Im}(f_0)_*, N_{\beta\gamma}}$$

by $\Phi([f]) = (\text{Im } f_*, N_f, [g])$. Here $[g] \in N_f \backslash G / C_G(\text{Im}(f_0)_*)$ is a unique element satisfying $g((f_0)_*(x))g^{-1} = (f_* \circ \iota_*)(x)$ for any $x \in \pi_1(\partial M \setminus P, *_\partial)$, where ι_* is a homomorphism induced by the inclusion $\iota: \partial M \setminus P \rightarrow M \setminus \Gamma$ and a choice of path connecting $*$ and $*_\partial$.

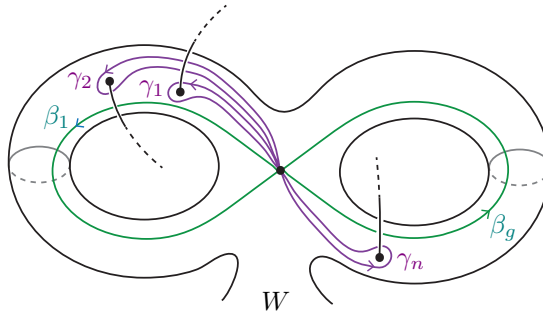


Figure 5: The oriented based loops $\beta_1, \dots, \beta_k, \gamma_1, \dots, \gamma_n$ on the boundary of the handlebody W .

If $f \sim f'$ via $\{h_t\}_t$, then we have a commutative diagram

$$\begin{array}{ccccc} \pi_1(M \setminus \widehat{\Gamma}) & \xrightarrow{\text{incl}_*} & \pi_1(M \setminus \Gamma) & \xrightarrow{f_*} & G \\ \downarrow h_1 \cong & & & & \parallel \\ \pi_1(M \setminus \widehat{\Gamma}') & \xrightarrow{\text{incl}_*} & \pi_1(M \setminus \Gamma') & \xrightarrow{f'_*} & G, \end{array}$$

and thus $\text{Im } f_* = \text{Im } f'_*$. The commutative diagram also implies that $N_f = N_{f'}$ and $f_* \circ \iota_* = f'_* \circ \iota_*: \pi_1(\partial M \setminus P, *_{\partial}) \rightarrow G$. Therefore, the map Φ is well-defined.

The main result of this paper is the following theorem, which gives the complete classification of defect configurations in handlebodies up to the above equivalence relation. Inspired by the approach taken in [20], we will reduce our claim to a statement about colored diagrams, Theorem 4.1 below.

Theorem 3.4. *The map Φ is a bijection.*

Note here that if M is a 3-ball and there are no boundary defects, then $N_f = \text{Im } f_*$ and $C_G(\text{Im}(f_0)_*) = G$ since $(f_0)_*$ is trivial, and thus $\mathcal{S}_{G, \text{Im}(f_0)_*, N_{\beta\gamma}}$ corresponds to $\mathcal{S}_G^{\text{fg}}$ in Section 2.4. Thus, Theorem 3.4 can naturally be thought of as a generalization of Theorem 2.4.

The next lemma enables us to describe continuous maps in terms of homomorphisms, which will be used in Section 4. Note that the freedom to define $f|_{\partial M}$ up to homotopy through the full X_G is essential here (cf. Remark 3.2).

Lemma 3.5. *The natural map (see Section 2.2)*

$$\theta: \text{Map}_0(M \setminus \Gamma, X_G; f_0)/\simeq \rightarrow \{\varphi \in \text{Hom}(\pi_1(M \setminus \Gamma, *), G) \mid \varphi \circ \iota_* \text{ is conjugate to } (f_0)_*\}$$

is a bijection, where $\iota: \partial M \setminus P \hookrightarrow M \setminus \Gamma$ is the inclusion and \simeq is the equivalence relation of basepoint-preserving homotopy.

Proof. First, note that we need to choose a path connecting $*$ and $*_{\partial}$ to define the induced homomorphism ι_* , but the condition on the right-hand side does not depend on the choice of that path. Let $K(G, 1)$ be an Eilenberg-MacLane space obtained from X_G by attaching cells of dimension greater than 3 (see the construction in [7, Section 4.2]). Since $M \setminus \Gamma$ is homotopy equivalent to a CW complex of dimension 2, the inclusion $X_G \subset K(G, 1)$ induces a bijection $\text{Map}_0(M \setminus \Gamma, X_G; f_0)/\simeq \rightarrow \text{Map}_0(M \setminus \Gamma, K(G, 1); f_0)/\simeq$. By a property of Eilenberg-MacLane spaces, the natural map $\text{Map}_0(M \setminus \Gamma, K(G, 1))/\simeq \rightarrow \text{Hom}(\pi_1(M \setminus \Gamma, *), G)$ is a bijection, and it restricts to the map θ on $\text{Map}_0(M \setminus \Gamma, X_G; f_0)/\simeq$. This shows that θ is injective.

Now it suffices to show the surjectivity of θ . Consider the following commutative diagram, where the horizontal arrows are bijections:

$$\begin{array}{ccc} \text{Map}_0(M \setminus \Gamma, K(G, 1))/\simeq & \xrightarrow{\quad} & \text{Hom}(\pi_1(M \setminus \Gamma, *), G) \\ \downarrow \iota_* & & \downarrow \iota_* \\ \text{Map}(\partial M \setminus P, K(G, 1))/\simeq & \xrightarrow{\theta'} & \text{Hom}(\pi_1(\partial M \setminus P, *_{\partial}), G)/\text{conj}, \end{array}$$

Let φ be an element of $\text{Hom}(\pi_1(M \setminus \Gamma, *), G)$ such that $\varphi \circ \iota_*$ is conjugate to $(f_0)_*$, and let $f: M \setminus \Gamma \rightarrow K(G, 1)$ be the corresponding continuous map (up to homotopy). Since the map θ' appearing in the diagram is a bijection, we have $[f \circ \iota] = \iota_*([f]) = [f_0]$, that is, the map $f \circ \iota$ is homotopic to f_0 . \square

3.2 Diagrammatic description

For a positive integer k , a k -rose is a graph consisting of a single vertex and k loops. For technical reasons, in this paper, we define a 0-rose to be an interval with a basepoint. We call a diagram of a spatial k -rose having no crossings the *standard diagram* of a spatial k -rose. Given the handlebody M of genus k as above, fix a deformation retraction of its exterior $\{h_t: W \rightarrow W\}_{t \in [0, 1]}$ onto a k -rose B such that $h_t|_{\partial M}$ is an embedding for $t \in [0, 1)$, h_1 sends $*_{\partial}$ to the unique vertex (basepoint) of the rose, and $h_1|_{P \cup \{*\}_{\partial}}$ is injective. We can identify $S^3 \setminus \text{Int } N(B)$ with $M = E(W)$, where $N(B)$ denotes a regular neighborhood of B . When a spatial graph Γ is given, we extend the edges incident to the boundary by h_t until they reach B and denote the resulting graph by Γ again. Then $S^3 \setminus (B \cup \Gamma)$ is homeomorphic to $\text{Int } M \setminus \Gamma$. Consider a diagram of the graph $B \cup \Gamma$ such that the subdiagram corresponding to B is standard, as on the right in Figure 6.

Let $\Lambda = \{\alpha_1, \dots, \alpha_k, \beta_1, \dots, \beta_k, \gamma_1, \dots, \gamma_n\}$ be oriented loops on ∂M , based at $*_{\partial}$, such that their images under h_{ε} are as illustrated in Figure 6 for $\varepsilon > 0$ small enough. The loops $\alpha_j, \beta_k, \gamma_l$ form a generating set for $\pi_1(\partial M \setminus P, *_{\partial})$. Note that, in the diagrammatic model illustrated on the right in Figure 6, the loops $\alpha_1, \dots, \alpha_g$ are not null-homotopic, although they may appear so—when we draw B , we really mean its ε -neighborhood $N(B)$ with basepoint on its boundary.

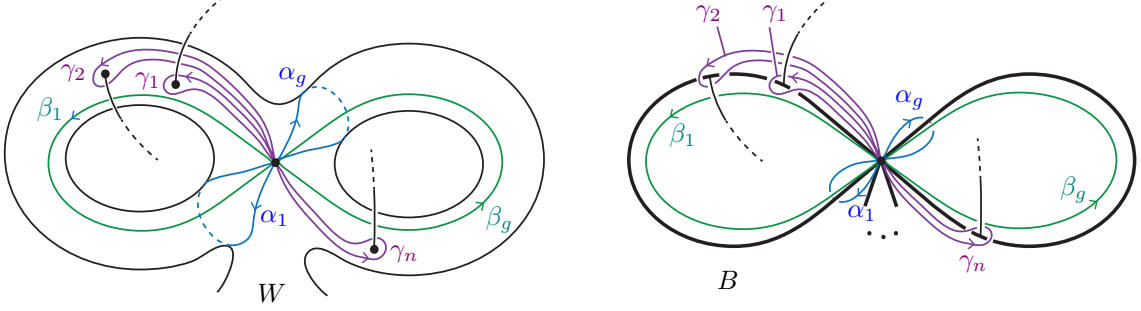


Figure 6: (Left) The oriented based loops $\alpha_1, \dots, \alpha_k, \beta_1, \dots, \beta_k, \gamma_1, \dots, \gamma_n$ on the boundary of the exterior handlebody W . (Right) Simplified version of the left figure, which will be used throughout the paper. Here, W is recovered from the bold rose B by thickening.

Definition 3.6. A G -colored oriented spatial graph diagram relative to f_0 (or simply, G -colored diagram rel f_0) is a diagram $D = D_B \cup D_{\Gamma}$ of an oriented spatial graph $B \cup \Gamma$ such that

- (1) each arc is colored by an element of G (we write $\text{col}(\alpha)$ for the color of an arc $\alpha \in \mathcal{A}_D$ of D);
- (2) at each crossing or vertex, the colors of the incident arcs satisfy the identities shown in Figure 7, which come from the Wirtinger relations; and

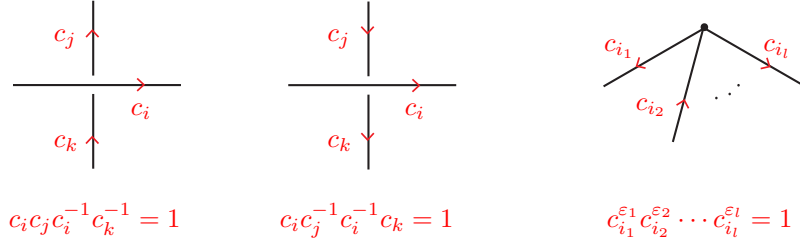


Figure 7: Colors around crossings and vertices.

- (3) there exists $g \in G$ such that, for each loop $\lambda \in \Lambda$, $g[f_0(\lambda)]g^{-1} = \prod_{\alpha} \text{col}(\alpha)^{\varepsilon_{\alpha}} \in G$, where α runs over all arcs crossing over λ and $\varepsilon_{\alpha} = 1$ (resp. $\varepsilon_{\alpha} = -1$) if the crossing is positive (resp. negative).

Note that g in (3) is unique as an element of $G/C_G(\text{Im}(f_0)_*)$. The left quotient appearing in the definition of $\mathcal{S}_{G, \text{Im}(f_0)_*, N_{\beta\gamma}}$ comes from the equivalence between diagrams.

Example 3.7. In Figure 8, the right-hand side of the identity in (3) for $\lambda = \gamma_2$ is $c_9^{-1} c_7 c_9$.

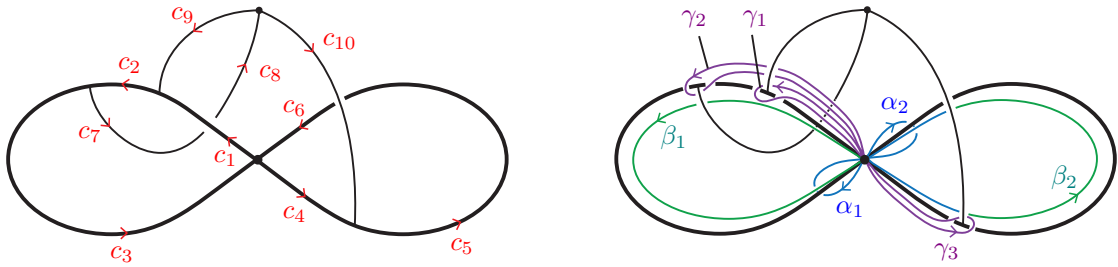


Figure 8: An example of a G -colored diagram for $k = 2$, $n = 3$, and the oriented loops.

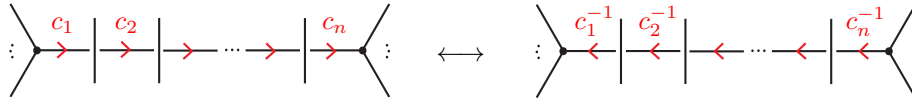


Figure 9: Orientation-reversal.

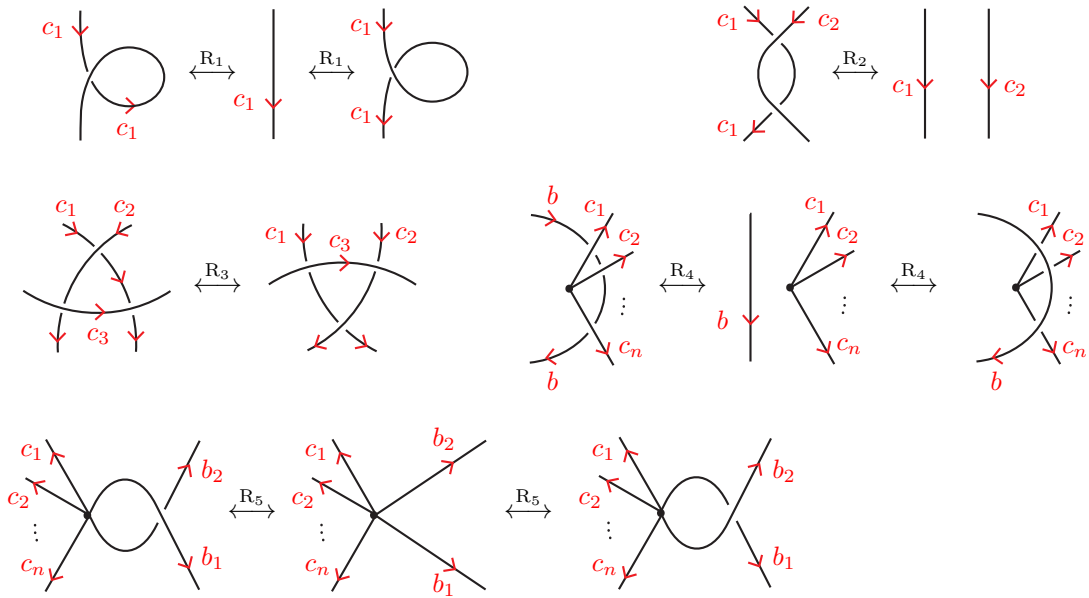


Figure 10: Reidemeister moves: The colors of the short ‘local’ arcs are omitted because they are uniquely determined by the colors of the other arcs, according to the appropriate Wirtinger relations.



Figure 11: The forbidden R_5 moves (left) and examples of (allowed) R_5 moves (right), where vertical bold lines are parts of B .

We here introduce local moves among G -colored diagrams $D = D_B \cup D_\Gamma$. The diagram D_B of the rose B is assumed to be fixed during those moves. See [20] for more detailed description.

- Definition 3.8.** (1) An *orientation-reversal* for D , which is described in Figure 9.
- (2) *Reidemeister moves* for D , which are described in Figure 10, except for the forbidden R_5 moves shown in Figure 11.
- (3) An *edge-contraction* or a *vertex-splitting* for D_Γ . As special cases, we obtain an *edge-contraction* or an *edge-subdivision*. See Figure 12.
- (4) An *edge-addition* or an *edge-deletion* for D_Γ , which are described in Figure 13.
- (5) A *vertex-addition* or a *vertex-deletion* for D_Γ , which adds or deltes an isolated vertex.
- (6) A *simultaneous conjugation* for D , which replaces all colors c_1, c_2, \dots, c_n with their conjugates $xc_1x^{-1}, xc_2x^{-1}, \dots, xc_nx^{-1}$ by a fixed element $x \in G$ simultaneously.

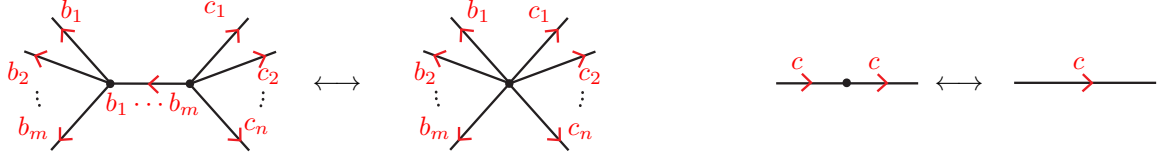


Figure 12: An edge-contraction and a vertex-splitting (left); an edge-combining and an edge-subdivision (right).

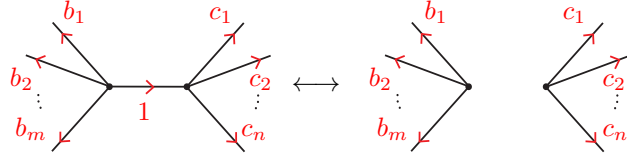


Figure 13: Edge-addition and edge-deletion.

4 Main results and examples

For a G -colored diagram D rel f_0 , let H_D denote the subgroup $\langle \text{col}(\alpha) \mid \alpha \in \mathcal{A}_{D_B \cup D_\Gamma} \rangle$ of G and let N_D denote the normal closure of $\{\text{col}(\alpha) \mid \alpha \in \mathcal{A}_{D_\Gamma}\}$ in H_D . One can define a map

$$\Psi: \{G\text{-colored diagrams rel } f_0\} / (1)-(5) \rightarrow \mathcal{S}_{G, \text{Im}(f_0)_*, N_{\beta\gamma}}$$

by $\Psi(D) = (H_D, N_D, [g])$, where g is an element appearing in Definition 3.6(3). Then, Ψ is well defined since H_D , N_D , and $[g]$ are invariant under moves (1)–(5). Note that move (2) changes g to hg for some $h \in N_D$ when an arc goes over the vertex of D_B , but these two elements are the same in $N_D \backslash G / C_G(\text{Im}(f_0)_*)$.

The map Ψ fits into a commutative diagram

$$\begin{array}{ccc} \{G\text{-colored diagrams rel } f_0\} / (1)-(5) & \xrightarrow{\Psi} & \mathcal{S}_{G, \text{Im}(f_0)_*, N_{\beta\gamma}} \\ \downarrow & \nearrow \Phi & \\ \left(\coprod_{\Gamma} \text{Map}_0(M \setminus \Gamma, X_G; f_0) \right) / \sim & & \end{array}$$

where the vertical map is induced by Lemma 3.5. Indeed, for a G -colored diagram D , we obtain an element of $\{\varphi \in \text{Hom}(\pi_1(M \setminus \Gamma, *), G) \mid (f_0)_* \text{ is conjugate to } \varphi \circ \iota_*\}$ due to the condition on colors in Definition 3.6, then Lemma 3.5 gives an element of $\text{Map}_0(M \setminus \Gamma, X_G; f_0) / \simeq$.

Theorem 4.1. *The map Ψ is a bijection.*

Now, Theorem 3.4 follows from Theorem 4.1 and the above commutative diagram. Indeed, Theorem 4.1 implies that the vertical map is a bijection, and hence Φ is also a bijection.

If we ignore basepoints, the above commutative diagram implies the following consequence.

Corollary 4.2. *The diagram*

$$\begin{array}{ccc} \{G\text{-colored diagrams rel } f_0\}/(1)\text{--}(6) & \xrightarrow{\Psi} & \mathcal{S}_{G, \text{Im}(f_0)_*, N_{\beta\gamma}}/\text{conj} \\ \downarrow & \nearrow \Phi & \\ \left(\coprod_{\Gamma} \text{Map}(M \setminus \Gamma, X_G; f_0)\right)/\sim & & \end{array}$$

is commutative, where the three maps are bijections. Here $\mathcal{S}_{G, \text{Im}(f_0)_*, N_{\beta\gamma}}/\text{conj}$ is the quotient set obtained by identifying $(H, N, [g])$ and $(H', N', [g'])$ if $(xHx^{-1}, xNx^{-1}, [xg]) = (H', N', [g'])$ for some $x \in G$.

Note that we have a bijection between $\mathcal{S}_{G, \text{Im}(f_0)_*, N_{\beta\gamma}}/\text{conj}$ and the set of pairs (H, N) up to conjugation by an element yz , where $y \in N$ and $z \in C_G(\text{Im}(f_0)_*)$.

Remark 4.3. Our classification of defects up to basepoint-preserving homotopy of ordered media in M also covers the case of defects in ordered media with constant far-field on the 3-dimensional space \mathbb{R}^3 outside of an unknotted handlebody (through one-point compactification of \mathbb{R}^3). The corollary covers the case of free homotopy of ordered media in the interior of an (unknotted) handlebody.

Example 4.4. Let $X_G = S^3/Q$, genus $k = 1$, and $P = \{p_1, p_2\}$. Fix a continuous map $f_0: \partial M \setminus \{p_1, p_2\} \rightarrow S^3/Q$ satisfying $(f_0)_*(\alpha_1) = (f_0)_*(\beta_1) = 1$, $(f_0)_*(\gamma_1) = i$, and $(f_0)_*(\gamma_2) = -i$. Then, $\text{Im}(f_0)_* = N_{\beta\gamma} = \langle i \rangle$, and thus $H = N$ for any $(H, N, [g]) \in \mathcal{S}_{Q, \langle i \rangle, \langle i \rangle}$. It follows that

$$\mathcal{S}_{Q, \langle i \rangle, \langle i \rangle} = \{(\langle i \rangle, \langle i \rangle, [1]), (\langle i \rangle, \langle i \rangle, [j]), (Q, Q, [1])\}.$$

Moreover, we have

$$\mathcal{S}_{Q, \langle i \rangle, \langle i \rangle}/\text{conj} = \{(\langle i \rangle, \langle i \rangle, [1]), (Q, Q, [1])\}.$$

Figure 14 shows a diagrammatic realization of each element of $\mathcal{S}_{Q, \langle i \rangle, \langle i \rangle}$. The configurations shown in the left and middle diagrams differ only by $[g]$. The defect configuration in the middle diagram can be obtained from that in the left diagram by dragging the image under f of a neighborhood of the basepoint $*$ along the loop in S^3/Q corresponding to j .

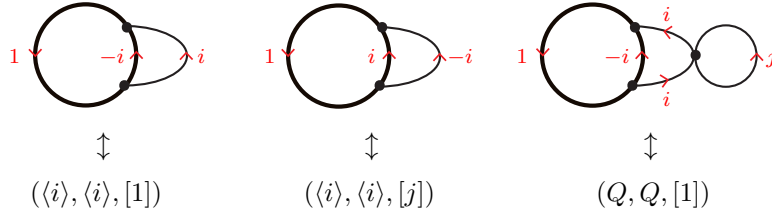


Figure 14: Three non-equivalent Q -colored diagrams rel f_0 .

In Appendix A, we give a complete classification, up to free homotopy, of non-trivial defects of a system defined on the solid torus $M = D^2 \times S^1$ that has S^3/Q as its order parameter space and no boundary defects such that the boundary condition is given by $f_0: \partial M \rightarrow S^3/Q$ with $(f_0)_*(\alpha) = i$.

5 Proof of Theorem 4.1

Recall that B is a k -rose in W with a fixed deformation retraction $\{h_t: W \rightarrow W\}_{t \in [0,1]}$ onto B such that $h_t|_{\partial W}$ is an embedding for $t \in [0, 1)$, h_1 sends $*_{\partial}$ to the unique vertex of the rose, and $h_1|_{P \cup \{*\}_{\partial}}$ is injective. Consider a diagram $D = D_B \cup D_{\Gamma}$ of the graph $B \cup \Gamma$ such that the subdiagram D_B corresponding to B is standard.

We say that a G -colored diagram D is in a *standard form* if it satisfies the following conditions (see Figure 15):

- D_{Γ} has a single vertex v_0 that does not touch D_B ;
- D_{Γ} has no self-crossings;
- for each edge of D_B , there exists a unique loop of D_{Γ} that is hooked to that edge, that is, the corresponding loop of Γ is freely homotopic to the meridian of the edge of B ;

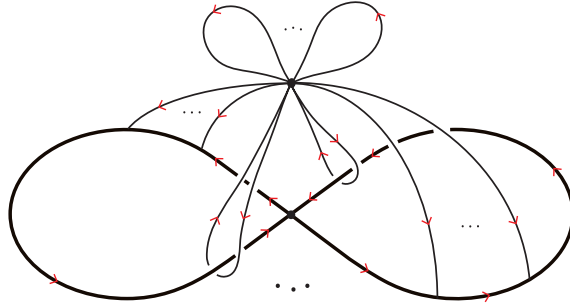


Figure 15: A Standard form of G -colored diagram, where the colors on edges are omitted.

- for each point of D_B corresponding to one of the boundary defects p_1, \dots, p_n , there is a unique edge of D_Γ connecting v_0 and that point; and
- at every crossing of D_B and D_Γ , except the hooks mentioned above, D_Γ crosses over D_B .

For a diagram $D = D_B \cup D_\Gamma$ in a standard form, we divide the edges of D_Γ into three as follows:

- the set $D_\Gamma^{(1)}$ of loops of D_Γ that are not hooked to an edge of D_B ;
- the set $D_\Gamma^{(2)}$ of loops of D_Γ that are hooked to an edge of D_B ; and
- the set $D_\Gamma^{(3)}$ of edges of D_Γ that are not loops.

Lemma 5.1. *Let $D = D_B \cup D_\Gamma$ be a G -colored diagram rel f_0 in a standard form. Then the colors of the arcs contained in the edges of $D_\Gamma^{(2)} \cup D_\Gamma^{(3)}$ are completely determined by f_0 and g defined in the condition (3) in Definition 3.6.*

Proof. The conditions (2) and (3) in Definition 3.6 provide equations in G relating the arc colors of $D_\Gamma^{(2)} \cup D_\Gamma^{(3)} \cup D_B$. The idea is to proceed inductively from the basepoint of D_B , solving these equations for the arc colors.

Consider, for example, a part of a G -colored diagram in a standard form shown in Figure 16. Then we have $gf_0(\alpha_1)g^{-1} = c_1$, which implies that c_1 is determined by f_0 and g . Since $c_2 = d_1c_1d_1^{-1}$,

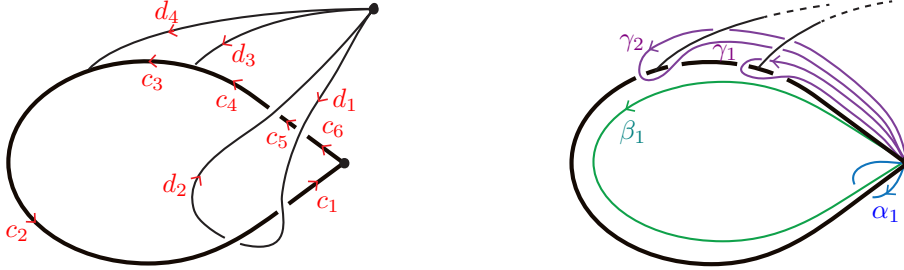


Figure 16: A part of a G -colored diagram in a standard form.

we can write $d_2 = c_2^{-1}d_1c_2 = d_1c_1^{-1}d_1c_1d_1^{-1}$. Thus, we have $g[f_0(\beta_1)]g^{-1} = d_1^{-1}d_2d_1 = c_1^{-1}d_1c_1$, which implies that d_1 is determined by f_0 and g . The equality $g[f_0(\beta_1)]g^{-1} = d_1^{-1}d_2d_1$ then implies that d_2 is also determined by f_0 . Since we have $g[f_0(\gamma_1)]g^{-1} = d_1^{-1}d_2d_3^{-1}d_2^{-1}d_1$, the color d_3 is determined by f_0 and g . Similarly, since $g[f_0(\gamma_2)]g^{-1} = d_1^{-1}d_2d_3^{-1}d_4^{-1}d_3d_2^{-1}d_1$, the color d_4 is also determined only by f_0 and g . Now, the remaining colors c_2, \dots, c_6 are determined from the other colors by the condition (2) in Definition 3.6. Consequently, all colors $c_1, \dots, c_6, d_1, \dots, d_4$ are determined by f_0 . The general case can be proved in the same way with additional indices. \square

Proof of Theorem 4.1. We first show the surjectivity of Ψ . Let $(H, N, [g]) \in \mathcal{S}_{G, \text{Im}(f_0)_*, N_{\beta_\gamma}}$, that is, $[g] \in N \backslash G / C_G(\text{Im}(f_0)_*)$, $g \text{Im}(f_0)_* g^{-1} \subset H$, $g N_{\beta_\gamma} g^{-1} \subset N$ and there exists a finite subset $T = \{c_1, \dots, c_m\}$ of N satisfying $\langle g \text{Im}(f_0)_* g^{-1} \cup T \rangle = H$ and $\langle\langle T \rangle\rangle_H = N$. We consider a (non-colored) diagram $D = D_B \cup D_\Gamma$ in a standard form such that the set $D_\Gamma^{(1)}$ consists of n loops. Color the loops of $D_\Gamma^{(1)}$ by $\{c_1, \dots, c_m\}$, respectively. By the arguments of Lemma 5.1, we can define the colors of the edges of $D_\Gamma^{(2)} \cup D_\Gamma^{(3)}$ automatically from f_0 and g . Then, the resulting G -colored

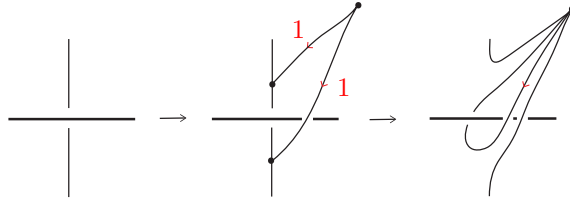


Figure 17: Adding two edges colored with 1 from the unique vertex to arcs crossing under D_B , and then contracting them.

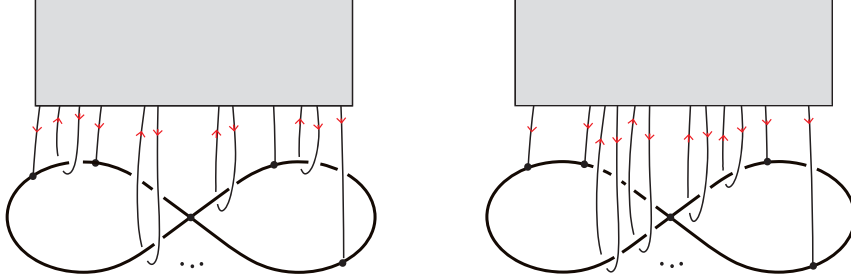


Figure 18: Simplification of colored graphs in the neighborhood of the k -rose B .

diagram D satisfies $\langle \text{col}(\alpha) \mid \alpha \in \mathcal{A}_D \rangle = H$ and $\langle\langle \{\text{col}(\alpha) \mid \alpha \in \mathcal{A}_{D_\Gamma}\} \cup T \rangle\rangle_H = N$. Thus D lies in the preimage $\Psi^{-1}(H, N, [g])$.

It remains to show that Ψ is injective. Choose $(H, N, [g]) \in \mathcal{S}_{G, \text{Im}(f_0)_*, N_{\beta\gamma}}$. Let $D = D_B \cup D_\Gamma$ be an arbitrary G -colored diagram $\text{rel } f_0$ in the preimage $\Psi^{-1}(H, N, [g])$. We show that by a sequence of local moves (1)–(5) for $D = D_B \cup D_\Gamma$ introduced in Section 3, D is transformed into a standard form. First, by adding edges colored by 1 appropriately, we can assume that a graph Γ corresponding to D_Γ is connected. Then, by contracting the edges of a maximal tree of Γ , we can assume that Γ has a single vertex, where the image of the vertex is on the top of the diagram. Furthermore, by applying the operations depicted in Figure 17 to each crossing where a strand of D_Γ passes under a strand of D_B , we obtain a diagram like that shown on the left of Figure 18, or more precisely, a diagram satisfying the following conditions:

- outside of the shaded box, D_Γ has no self-crossings;
- for each point of D_B corresponding to one of the boundary defects p_1, \dots, p_n , there is a portion of an edge of D_Γ extending from the shaded box to that point;
- each portion of D_Γ 's edges outside of the shaded box, apart from those arcs described above, is hooked to an edge of D_B so that if we contract the shaded box to a point, that portion represents a loop that is freely homotopic to the meridian of the corresponding edge of D_B ; and
- at every crossing of D_B and D_Γ , except for the hooks mentioned above, D_Γ crosses over D_B .

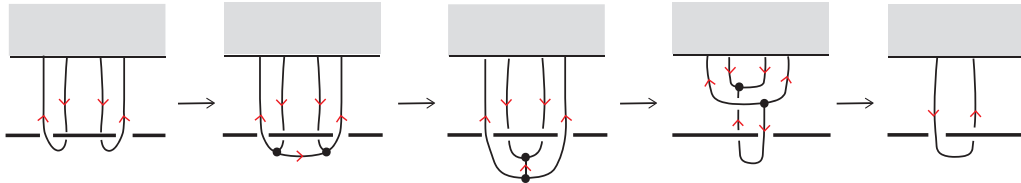


Figure 19: A sequence of moves that reduces the number of loops hooked to an edge of D_B .

By the moves (1)–(5) in Definition 3.8, the images of the loops of Γ hooked to each edge of D_B can be collected in one place as shown on the right in Figure 18. Then, after applying the moves shown in Figure 19 finitely many times, we may assume that for each edge of D_B , there exists a unique loop of D_Γ that is hooked to that edge.

Now, the diagram is in a standard form outside of the grayed-out box. The remaining argument to get a standard form is similar to that of Nozaki et al. [20]. Indeed, the move shown in Figure 20 replaces a crossing with a vertex; thus, we can assume that the diagram D_Γ has no self-crossings. By contracting edges to get a diagram with a single vertex, we finally obtain a diagram in a standard form.

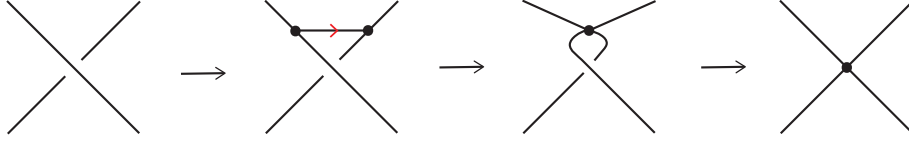


Figure 20: A sequence of moves changing a crossing to a vertex.

Let $D = D_B \cup D_\Gamma$ and $D' = D_B \cup D_{\Gamma'}$ be G -colored diagrams in standard form satisfying $\Psi(D) = \Psi(D') = (H, N, [g])$. Let g and g' be elements of G defined in the condition (3) in Definition 3.6 for D and D' , respectively. Then, $hgs = g'$ for some $h \in N$ and $s \in C_G(\text{Im}(f_0)_*)$. Figure 21 enables us to create a loop colored by h . Following Figure 22, we can transform D' to another standard form D'' such that $g'' = h^{-1}g' = gs$.

Clearly, the number of edges of $D_\Gamma^{(2)}$ and $D_{\Gamma'}^{(2)}$ as well as $D_\Gamma^{(3)}$ and $D_{\Gamma'}^{(3)}$ are the same. Further, by Lemma 5.1, the colors of the arcs in $D_\Gamma^{(2)} \cup D_{\Gamma'}^{(2)}$ and $D_\Gamma^{(3)} \cup D_{\Gamma'}^{(3)}$ are automatically determined by f_0, g and f_0, gs , respectively. Since $s \in C_G(\text{Im}(f_0)_*)$, it does not affect this process. Finally, since $N_D = N = N_{D'}$, we can deform $D_{\Gamma'}^{(1)}$ into $D_\Gamma^{(1)}$ using [20, Figure 16]. Therefore, $D = D'$ up to the moves (1)–(5). \square

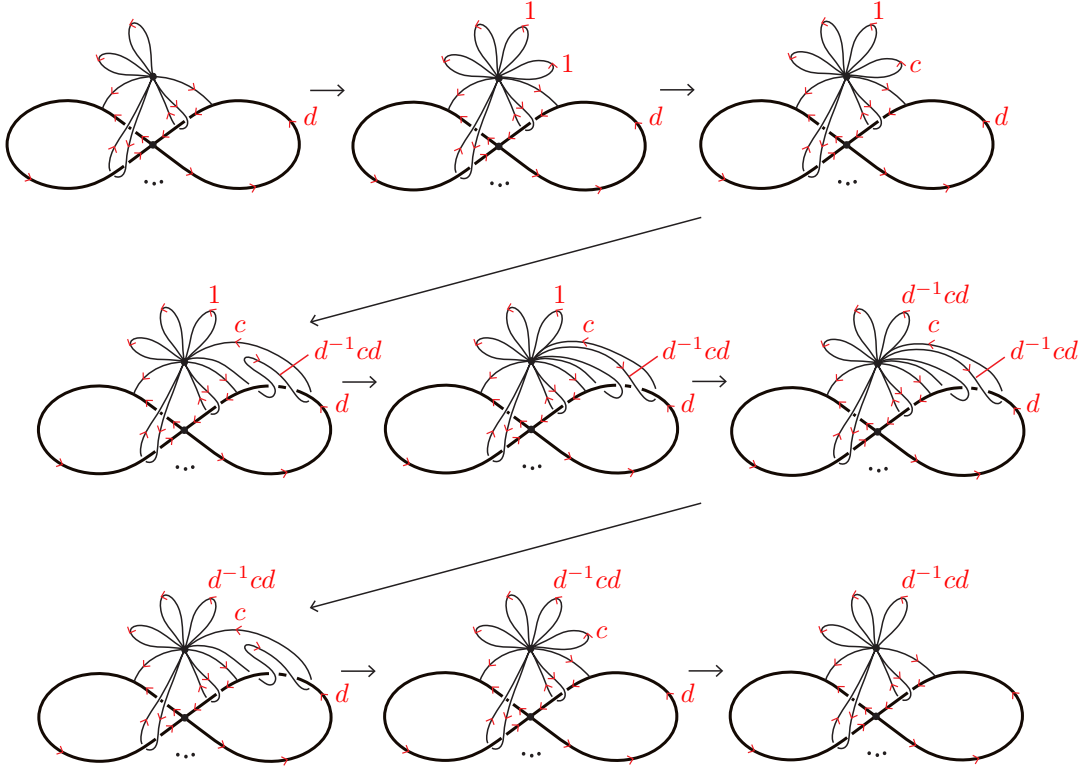


Figure 21: A sequence of moves creating a loop colored by $d^{-1}cd$, where $c \in \{\text{col}(\alpha) \mid \alpha \in \mathcal{A}_{D_\Gamma'}\}$ and $d \in H = \langle \text{col}(\alpha) \mid \alpha \in \mathcal{A}_{D_B \cup D_{\Gamma'}} \rangle$. Here, the second and eighth (resp. fifth) moves follow from Figure 16 (resp. Figure 13) in [20].

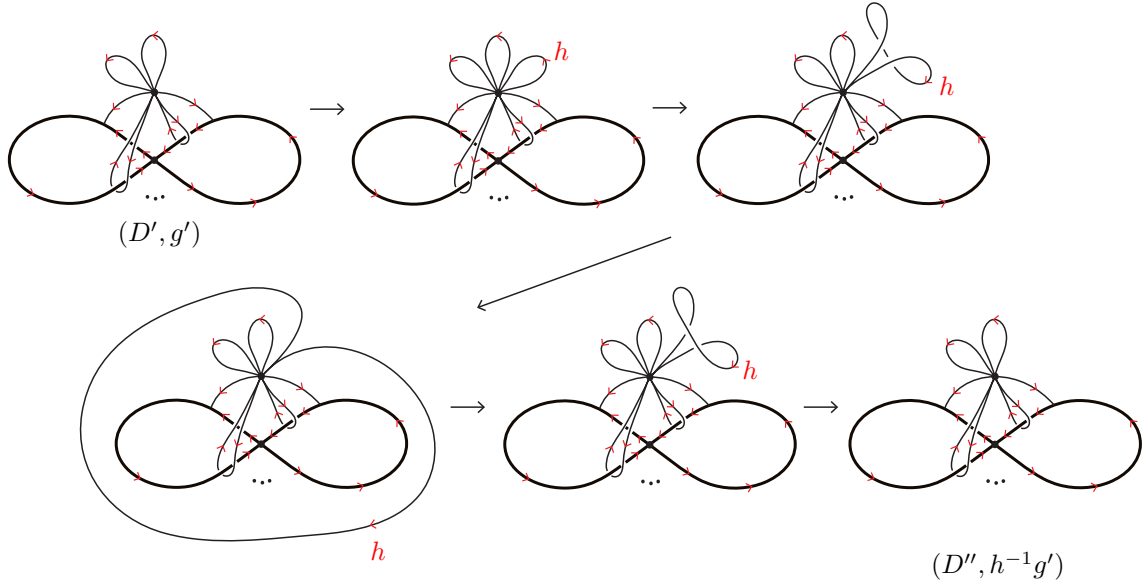


Figure 22: A sequence of moves changing g' to $h^{-1}g'$ in Definition 3.6(3).

A Classification example: a system on the solid torus with order parameter space S^3/Q and no boundary defects

Let $X_G = S^3/Q$, $k = 1$ and $P = \emptyset$, that is, we are considering a system defined on the solid torus $M = D^2 \times S^1$ that has S^3/Q as its order parameter space and no boundary defects. Then $\pi_1(\partial M, *_{\partial})$ is the free abelian group of rank two generated by the loops $\alpha = \alpha_1$ and $\beta = \beta_1$. Let $f_0: \partial M \rightarrow S^3/Q$ satisfy $(f_0)_*(\alpha) = i \in Q$. We can classify the equivalence classes of global defect configurations with the boundary condition f_0 as follows.

Suppose first that $(f_0)_*(\beta) = 1$. Then, we have $\mathcal{S}_{G, \text{Im}(f_0)_*, N_{\beta\gamma}} = \mathcal{S}_{Q, \langle i \rangle, \{1\}}$. As we have seen in Example 3.3, this set consists of nine elements, and from this, we can check easily that $\mathcal{S}_{Q, \langle i \rangle, \{1\}}/\text{conj}$ consists of six elements (see Corollary 4.2). The element $(\langle i \rangle, \{1\}, [1])$ corresponds to the empty defect, and we can choose a representative of the equivalence class of colored diagrams corresponding to each of the other five elements as shown in Figure 23.

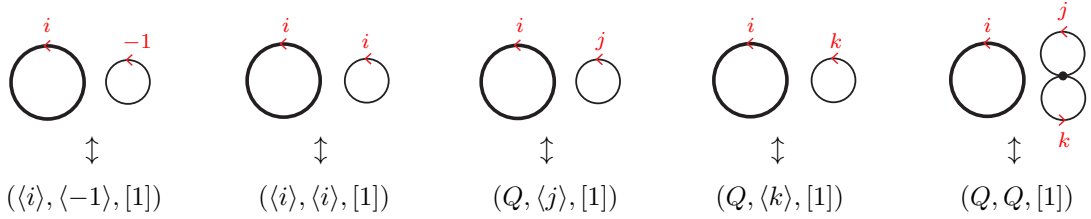


Figure 23: Representatives of the equivalence classes of colored diagrams corresponding to non-trivial elements of $\mathcal{S}_{Q, \langle i \rangle, \{1\}}/\text{conj}$ in the case where $(f_0)_*(\beta) = 1$.

Next, suppose that $(f_0)_*(\beta) = -1$. Then, we have $\mathcal{S}_{G, \text{Im}(f_0)_*, N_{\beta\gamma}} = \mathcal{S}_{Q, \langle i \rangle, \langle -1 \rangle}$. As we have seen in Example 3.3, this set consists of seven elements, and from this, we see that $\mathcal{S}_{Q, \langle i \rangle, \langle -1 \rangle}/\text{conj}$ consists of five elements, where a representative of the equivalence class of colored diagrams corresponding to each of those elements can be seen in Figure 24.

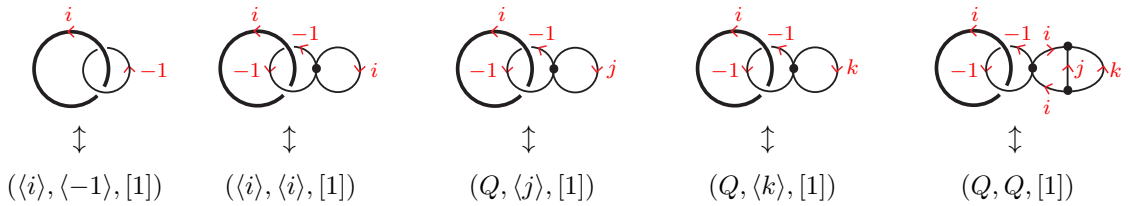


Figure 24: Representatives of the equivalence classes of colored diagrams corresponding to elements of $\mathcal{S}_{Q, \langle i \rangle, \langle -1 \rangle}/\text{conj}$ in the case where $(f_0)_*(\beta) = -1$.

Finally, suppose that $(f_0)_*(\beta) = \pm i$. In this case, we have $\mathcal{S}_{G, \text{Im}(f_0)_*, N_{\beta\gamma}} = \mathcal{S}_{Q, \langle i \rangle, \langle i \rangle}$. As we have seen in Example 3.3, this set consists of three elements, and from this, we see that $\mathcal{S}_{Q, \langle i \rangle, \{1\}}/\text{conj}$ consists of two elements. A representative of the equivalence class of colored diagrams corresponding to each of those elements for $(f_0)_*(\beta) = \pm i$ can be seen in Figure 25.



Figure 25: Representatives of the equivalence classes of colored diagrams corresponding to elements of $\mathcal{S}_{Q, \langle i \rangle, \langle i \rangle}/\text{conj}$ in the case where $(f_0)_*(\beta) = i$ (left) or $(f_0)_*(\beta) = -i$ (right).

Note that the list of representatives of the colored diagrams obtained above is exactly the one we introduced in Section 1 with Figure 2. By Corollary 4.2, this gives a complete classification, up to free homotopy, of non-trivial defect configurations of a system defined on the solid torus M with order parameter space S^3/Q and no boundary defects, subject to the boundary condition $f_0: \partial M \rightarrow S^3/Q$ with $(f_0)_*(\alpha) = i$.

Obviously, there are infinitely many colored diagrams in each equivalence class of colored diagrams. For example, the equivalence class of colored diagrams corresponding to the element $(\langle i \rangle, \langle i \rangle, [1])$ of $\mathcal{S}_{Q, \langle i \rangle, \langle -1 \rangle}/\text{conj}$ contains the colored diagrams depicted in Figure 26. Similarly, the

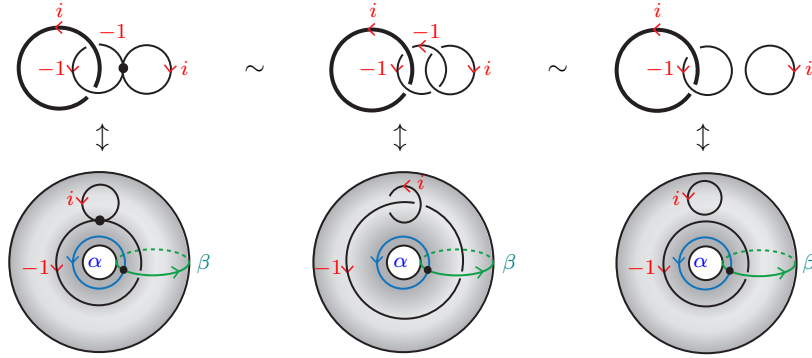


Figure 26: Some equivalent colored diagrams corresponding to the element $(\langle i \rangle, \langle i \rangle, [1])$ of $\mathcal{S}_{Q, \langle i \rangle, \langle -1 \rangle}/\text{conj}$.

three colored diagrams depicted in Figure 27 belong to the same equivalence class because they all correspond to the same element $(Q, Q, [1])$ of $\mathcal{S}_{Q, \langle i \rangle, \langle i \rangle}/\text{conj}$. Using Corollary 4.2, we can determine

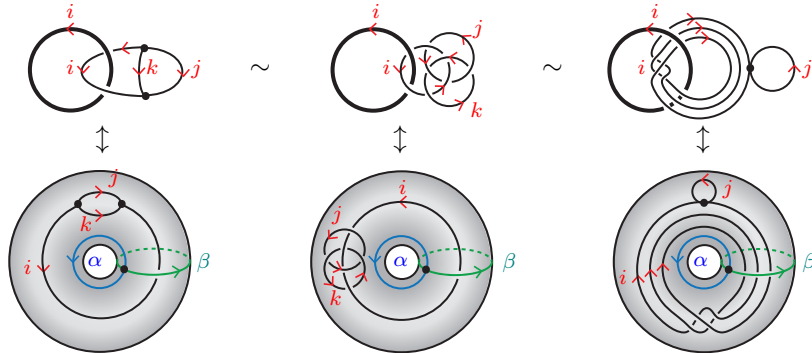


Figure 27: Some equivalent colored diagrams corresponding to the element $(Q, Q, [1])$ of $\mathcal{S}_{Q, \langle i \rangle, \langle i \rangle}/\text{conj}$.

whether two diagrams of defect configurations are equivalent by simply comparing the corresponding elements of $\mathcal{S}_{G, \text{Im}(f_0)_*, N_{\beta\gamma}}/\text{conj}$, which are easily computed from the diagrams.

B The subgroups of the binary octahedral group $2O$

The following is the list of all subgroups of $2O$.

- Subgroups of Q .
 - (i) $\{1\} = \langle 1 \rangle$.
 - (ii) $\langle -1 \rangle \cong \mathbb{Z}/2\mathbb{Z}$.
 - (iii) $\langle i \rangle \cong \mathbb{Z}/4\mathbb{Z}$, $\langle j \rangle$, $\langle k \rangle$.
 - (iv) (**order 8**) $Q = \langle i, j \rangle$.
- Subgroups of $2T$ not contained in Q .
 - (v) $\langle c^2 \rangle = \{1, c^2, ct = -c\} \cong \mathbb{Z}/3\mathbb{Z}$, $\langle \alpha^2 \rangle$, $\langle \beta^2 \rangle$, $\langle \gamma^2 \rangle$.
 - (vi) $\langle c \rangle = \{\pm 1, \pm c, \pm c^2\} \cong \mathbb{Z}/6\mathbb{Z}$, $\langle \alpha \rangle$, $\langle \beta \rangle$, $\langle \gamma \rangle$.
 - (vii) $2T = \langle i, c \rangle$.
- Subgroups of $2O$ not contained in $2T$.
 - (viii) $\langle \frac{1}{\sqrt{2}}(i+j) \rangle = \left\{ \pm 1, \pm \frac{1}{\sqrt{2}}(i+j) \right\} \cong \mathbb{Z}/4\mathbb{Z}$, $\langle \frac{1}{\sqrt{2}}(j+k) \rangle$, $\langle \frac{1}{\sqrt{2}}(k+i) \rangle$, $\langle \frac{1}{\sqrt{2}}(i-j) \rangle = \left\{ \pm 1, \pm \frac{1}{\sqrt{2}}(i-j) \right\}$, $\langle \frac{1}{\sqrt{2}}(j-k) \rangle$, $\langle \frac{1}{\sqrt{2}}(k-i) \rangle$.
 - (ix) $\langle \frac{1}{\sqrt{2}}(1+i) \rangle = \left\{ \pm 1, \pm i, \frac{1}{\sqrt{2}}(\pm 1, \pm i) \right\}$, $\langle \frac{1}{\sqrt{2}}(1+j) \rangle \cong \mathbb{Z}/8\mathbb{Z}$, $\langle \frac{1}{\sqrt{2}}(1+k) \rangle$.
 - (x) $Q_8(i) := \langle i, \frac{1}{\sqrt{2}}(j+k) \rangle = \left\{ \pm 1, \pm i, \frac{1}{\sqrt{2}}(j+k), \pm \frac{1}{\sqrt{2}}(j-k) \right\} \cong Q \cong D_2^*$, $Q_8(j) := \langle j, \frac{1}{\sqrt{2}}(k+i) \rangle$, $Q_8(k) := \langle k, \frac{1}{\sqrt{2}}(i+j) \rangle$.
 - (xi) $Q_{12}(c) := \langle c, \frac{1}{\sqrt{2}}(i-j) \rangle = \left\{ \pm 1, \pm c, \pm c^2, \pm \frac{1}{\sqrt{2}}(i-j), \pm \frac{1}{\sqrt{2}}(j-k), \pm \frac{1}{\sqrt{2}}(k-i) \right\} \cong D_3^*$,
 $Q_{12}(\alpha) := \langle \alpha, \frac{1}{\sqrt{2}}(i+j) \rangle = \left\{ \pm 1, \pm \alpha, \pm \alpha^2, \pm \frac{1}{\sqrt{2}}(i+j), \pm \frac{1}{\sqrt{2}}(j-k), \pm \frac{1}{\sqrt{2}}(k+i) \right\}$, $Q_{12}(\beta)$,
 $Q_{12}(\beta)$.
 - (xii) $Q_{16}(i) := \langle i, \frac{1}{\sqrt{2}}(1+k) \rangle = Q \cup \left\{ \frac{1}{\sqrt{2}}(\pm i \pm j), \pm \frac{1}{\sqrt{2}}(\pm 1 \pm k) \right\} \cong D_4^*$, $Q_{16}(j)$, $Q_{16}(k)$.
 - (xiii) $2O = \langle c, \frac{1}{\sqrt{2}}(i+j) \rangle$.

The subgroups within each item of the above list are conjugate to each other. Thus, only $\{1\}$, $\langle -1 \rangle$, Q , $2T$ and $2O$ are normal subgroups of $2O$, and there are totally thirteen conjugacy classes of subgroups.

References

- [1] Toni Annala, Hermanni Rajamäki, and Mikko Möttönen. “Bordism Invariants of Colored Links and Topologically Protected Tricolorings”. In: *Comm. Math. Phys.* 405.7 (2024), Paper No. 169. ISSN: 0010-3616. DOI: 10.1007/s00220-024-05058-8.
- [2] Toni Annala, Roberto Zamora-Zamora, and Mikko Möttönen. “Topologically protected vortex knots and links”. In: *Communications Physics* 5.1 (Dec. 12, 2022), p. 309. DOI: 10.1038/s42005-022-01071-2.
- [3] Alexandre Chemin, François Henrotte, Jean-François Remacle, and Jean Van Schaftingen. “Representing Three-Dimensional Cross Fields Using Fourth Order Tensors”. In: *27th International Meshing Roundtable*. Ed. by Xevi Roca and Adrien Loseille. Cham: Springer International Publishing, 2019, pp. 89–108. ISBN: 978-3-030-13992-6. DOI: 10.1007/978-3-030-13992-6_6.
- [4] Guillaume Coiffier and Etienne Corman. “The Method of Moving Frames for Surface Global Parametrization”. In: *ACM Transactions on Graphics* 42.5 (Sept. 20, 2023), 166:1–166:18. ISSN: 0730-0301. DOI: 10.1145/3604282.
- [5] Etienne Corman and Keenan Crane. “Symmetric Moving Frames”. In: *ACM Transactions on Graphics* 38.4 (July 12, 2019), 87:1–87:16. ISSN: 0730-0301. DOI: 10.1145/3306346.3323029.

- [6] Dmitry Golovaty, Jose Alberto Montero, and Daniel Spirn. “A Variational Method for Generating n -Cross Fields Using Higher-Order Q -Tensors”. In: *SIAM Journal on Scientific Computing* 43.5 (Jan. 2021), A3269–A3304. ISSN: 1064-8275. DOI: 10.1137/19M1287857.
- [7] Allen Hatcher. *Algebraic topology*. Cambridge University Press, Cambridge, 2002, pp. xii+544. ISBN: 0-521-79160-X; 0-521-79540-0.
- [8] A. Holz. “Topological Properties of Static and Dynamic Defect Configurations in Ordered Liquids”. In: *Physica A: Statistical Mechanics and its Applications* 182.1-2 (Mar. 1992), pp. 240–278. ISSN: 03784371. DOI: 10.1016/0378-4371(92)90241-H.
- [9] Jin Huang, Yiyong Tong, Hongyu Wei, and Hujun Bao. “Boundary Aligned Smooth 3D Cross-Frame Field”. In: *ACM Transactions on Graphics* 30.6 (Dec. 12, 2011), pp. 1–8. ISSN: 0730-0301. DOI: 10.1145/2070781.2024177.
- [10] Tengfei Jiang, Jin Huang, Yuanzhen Wang, Yiyong Tong, and Hujun Bao. “Frame Field Singularity Correction for Automatic Hexahedralization”. In: *IEEE Transactions on Visualization and Computer Graphics* 20.8 (Aug. 1, 2014), pp. 1189–1199. ISSN: 1077-2626. DOI: 10.1109/TVCG.2013.250.
- [11] Akio Kawachi, ed. *A survey of knot theory*. Translated and revised from the 1990 Japanese original by the author. Birkhäuser Verlag, Basel, 1996, pp. xxii+420. ISBN: 3-7643-5124-1.
- [12] Yufei Li, Yang Liu, Weiwei Xu, Wenping Wang, and Baining Guo. “All-Hex Meshing Using Singularity-Restricted Field”. In: *ACM Transactions on Graphics* 31.6 (Nov. 1, 2012), 177:1–177:11. ISSN: 0730-0301. DOI: 10.1145/2366145.2366196.
- [13] Heng Liu and David Bommes. “Locally Meshable Frame Fields”. In: *ACM Transactions on Graphics* 42.4 (July 26, 2023), 112:1–112:20. ISSN: 0730-0301. DOI: 10.1145/3592457.
- [14] Heng Liu, Paul Zhang, Edward Chien, Justin Solomon, and David Bommes. “Singularity-Constrained Octahedral Fields for Hexahedral Meshing”. In: *ACM Transactions on Graphics* 37.4 (Aug. 31, 2018), pp. 1–17. ISSN: 0730-0301, 1557-7368. DOI: 10.1145/3197517.3201344.
- [15] Thomas Machon and Gareth P. Alexander. “Knotted Defects in Nematic Liquid Crystals”. In: *Phys. Rev. Lett.* 113 (2 July 2014), p. 027801. DOI: 10.1103/PhysRevLett.113.027801.
- [16] Thomas Machon and Gareth P. Alexander. “Global defect topology in nematic liquid crystals”. In: *Proceedings of the Royal Society A: Mathematical, Physical and Engineering Sciences* 472.2191 (2016), p. 20160265. DOI: 10.1098/rspa.2016.0265.
- [17] N. D. Mermin. “The topological theory of defects in ordered media”. In: *Rev. Mod. Phys.* 51 (3 July 1979), pp. 591–648. DOI: 10.1103/RevModPhys.51.591.
- [18] Hiizu Nakanishi, Kiyoshi Hayashi, and Hiroyuki Mori. “Topological classification of unknotted ring defects”. In: *Comm. Math. Phys.* 117.2 (1988), pp. 203–213. ISSN: 0010-3616.
- [19] M. Nieser, U. Reitebuch, and K. Polthier. “CubeCover – Parameterization of 3D Volumes”. In: *Computer Graphics Forum* 30.5 (2011), pp. 1397–1406. ISSN: 1467-8659. DOI: 10.1111/j.1467-8659.2011.02014.x.
- [20] Y. Nozaki, T. Kálmán, M. Teragaito, and Y. Koda. “Homotopy classification of knotted defects in ordered media”. In: *Proceedings of the Royal Society A: Mathematical, Physical and Engineering Sciences* 480.2300 (2024), p. 20240148. DOI: 10.1098/rspa.2024.0148.
- [21] David Palmer, David Bommes, and Justin Solomon. “Algebraic Representations for Volumetric Frame Fields”. In: *ACM Trans. Graph.* 39.2 (Apr. 2020). ISSN: 0730-0301. DOI: 10.1145/3366786.
- [22] V. Poénaru. “Some aspects of the theory of defects of ordered media and gauge fields related to foliations”. In: *Comm. Math. Phys.* 80.1 (1981), pp. 127–136. ISSN: 0010-3616.
- [23] V. Poénaru and G. Toulouse. “The crossing of defects in ordered media and the topology of 3-manifolds”. In: *J. Physique* 38.8 (1977), pp. 887–895. ISSN: 0302-0738. DOI: 10.1051/jphys:01977003808088700.
- [24] Nicolas Ray, Dmitry Sokolov, and Bruno Lévy. “Practical 3D Frame Field Generation”. In: *ACM Transactions on Graphics* 35.6 (Dec. 5, 2016), 233:1–233:9. ISSN: 0730-0301. DOI: 10.1145/2980179.2982408.
- [25] Bohdan Senyuk, Cuiling Meng, and Ivan I. Smalyukh. “Design and Preparation of Nematic Colloidal Particles”. In: *Langmuir* 38.30 (Aug. 2, 2022), pp. 9099–9118. ISSN: 0743-7463. DOI: 10.1021/acs.langmuir.2c00611.

- [26] Zhongwei Shen, Xianzhong Fang, Xinguo Liu, Hujun Bao, and Jin Huang. “Harmonic Functions for Rotational Symmetry Vector Fields”. In: *Computer Graphics Forum* 35.7 (2016), pp. 507–516. ISSN: 1467-8659. DOI: 10.1111/cgf.13047.
- [27] Jung-Shen B. Tai and Ivan I. Smalyukh. “Surface Anchoring as a Control Parameter for Stabilizing Torons, Skyrmions, Twisted Walls, Fingers, and Their Hybrids in Chiral Nematics”. In: *Physical Review E* 101.4 (Apr. 30, 2020), p. 042702. DOI: 10.1103/PhysRevE.101.042702.
- [28] Carsten Tschierske and Demetri J. Photinos. “Biaxial Nematic Phases”. In: *Journal of Materials Chemistry* 20.21 (May 18, 2010), pp. 4263–4294. ISSN: 1364-5501. DOI: 10.1039/B924810B.
- [29] G. E. Volovik and V. P. Mineev. “Investigation of singularities in superfluid He³ in liquid crystals by homotopic topology methods”. In: *Ž. Èksper. Teoret. Fiz.* 72.6 (1977), pp. 2256–2274.
- [30] Tianyi Yao, Žiga Kos, Qi Xing Zhang, Yimin Luo, Francesca Serra, Edward B. Steager, Miha Ravnik, and Kathleen J. Stebe. “Nematic Colloidal Micro-Robots as Physically Intelligent Systems”. In: *Advanced Functional Materials* 32.44 (2022), p. 2205546. ISSN: 1616-3028. DOI: 10.1002/adfm.202205546.